Calibration of HPGe Well-type Detectors using the Direct Mathematical method

Mahmoud I. Abbas[1], Sherif S. Nafee[1, 2]and Younis S. Selim[1]

1. *Physics Department, Faculty of Science, Alexandria University: Moharem Bey St., Alexandria 21121, Egypt.*
2. *Ionizing Radiation Division, National Institute of Standards and Technology (NIST): 100 Bureau Dr./84602, Gaithersburg, Md 20899, U.S.A., Sherif.Nafee@nist.gov*

Abstract

A new theoretical approach is presented here to calibrate the HPGe well-type detectors using cylindrical sources. This approach depends on the accurate calculation of two important factors; the first factor is the average path length ($\bar{d}$) covered by the photon inside the active volume of a gamma detector, whereas, the second one is the geometrical solid angle (Ω_{geo}) subtended by the source to the detector. These two factors are theoretically derived in straightforward analytical formulae. The present model leads to a direct evaluation of the full energy peak efficiency (ε_P) for these source-detector geometries. The validity of this work will be clear via systematic comparisons for these geometries with the experimental method and the Monte Carlo simulations. Also the validity of it over the traditional direct mathematical method reported by Abbas [1] and Abbas and Selim [2] will be presented. Simple programming is possible and short computer time is needed.

INTRODUCTION

Well-type NaI (Tl) and HPGe crystals are very useful in low level gamma activity measurements due to the near 4π solid angle that can be obtained with them. Recently, absolute cross-sections for neutron-induced activation have been measured by gamma activity methods using such crystals by Jeronymo et al., [3]. They had indicated a method for absolute calibration of well-type crystals and problems connected with it. Based on this method, Redon et al., [4] measured the absolute (ε_P) as well as the resolution as a function of gamma energy.

In the applications of well-type crystals, the measurement of gamma activity induced in samples due to fast neutron bombardment is not constant along the length of the sample, so the variation of the crystal efficiency as a function of well depth as well as the self absorption of gamma rays by the sample, which reduces the values of the absolute efficiencies of the measured system must be known.

To determine the sample activity, the (ε_P) is needed. The computations of the well-type NaI(Tl) and HPGe detectors efficiencies have been reported in literatures [5-11]. In the present work we introduce a new technique involving the determination of the average path length ($\bar{d}$) covered by a photon inside the detector active volume and the geometrical solid angle (Ω_{geo}), which is defined as the angle subtended by the detector at the source point, by using a direct mathematical formula in three different cases (axial point, non-axial point and cylindrical sources).

Mathematical View Point

The full-energy peak efficiency (ε_p) for any source-detector geometry is defined as a product of the geometrical efficiency (ε_g) and the intrinsic full-energy peak efficiency (ε_{ip}), which were treated mathematically by Selim and Abbas [12, 13]. Then, for an arbitrarily positioned radiating point source placed at any distance from the internal bottom of a well-type detector shown in Fig. 1, (ε_p) can be represented by the following equation:

$$\varepsilon_{point} = \frac{\Omega}{4\pi}\left(1 - e^{-\mu.\bar{d}}\right) \tag{1}$$

The first and the second terms in equation (1) represent the geometrical and the intrinsic efficiencies, respectively, and ($\bar{d}$) for an isotropic emission from the source is given as:

$$\bar{d} = \frac{\int_{\Omega}(\sum_{j=1}^{n} d_j)\, d\Omega}{\int_{\Omega} d\Omega} = \frac{\int_{\theta}\int_{\phi}(\sum_{j=1}^{n} d_j)\sin\theta\, d\phi\, d\theta}{\Omega} \tag{2}$$

where d_1, d_2, ……, d_n are the possible photon path lengths traveled within the detector active volume (we will discuss them in details below). In equation (2), the numerator represents the integration of all possible gamma-ray paths in the detector over the subtended solid angle by the detector to the source, and the denominator represents the solid angle, which is given as:

$$\Omega = \int_{\phi}\int_{\theta}\sin(\theta)\, d\theta\, d\phi \tag{3}$$

In equation (1), (θ) and (ϕ) are the polar and the azimuthal angle, respectively. μ is the attenuation coefficient of the detector's material. For calculating (ε_p), μ should be replaced by the full-energy peak attenuation coefficient (μ_P) for the detector's material, which represents the only part contributing to the full-energy peak (the photoelectric coefficient + the fractions of the Compton and pair production coefficients which represent the photons that have enough energy to make photoelectric interaction and subsequently deposit its energy under the full-energy peak). The calculated fractions are given in details in [14].

For the extended volumetric sources, equation (1) must be multiplied by a factor (f_{att}) which determines the photon attenuation by the source container, the window and the detector's end cap materials and is expressed as:

$$f_{att} = e^{-\sum_i \mu_i \delta_i} \tag{4}$$

where, μ_i is the total attenuation coefficient with coherent scattering of the i^{th} absorber for a gamma-ray photon with energy E_γ [15] and (δ_i) is the possible path length of the gamma photon through the i^{th} absorber.

The calculations of ($\bar{d}$) and (Ω) depend on the source-detector positions. We have two main cases to be considered. The first case has two sub-cases to describe the axial position of the isotropic radiating point source, shown in Fig. 2, whereas, the second one has three sub-cases to describe the non-axial position of the source, shown in Fig. 3.

The Case of an Axial-Point Source

If an arbitrarily positioned isotropic radiating point source is placed on the axis of a well-type detector at a distance h' from the bottom$_1$, see (Fig. 2). Each striking photon may enter from the detector's bottom$_1$ or from the detector's side$^+_1$ (or side$^-_1$). The two cases are described as:

1- If the photon enters from the detector's bottom$_1$, it may emerge from its bottom$_2$ or from its side$_2$. The distances traveled by the photon in both cases are given by the following equations:

$$d_1 = \frac{L}{\cos\theta} \quad \text{and} \quad d_2 = \frac{R_\circ}{\sin\theta} - \frac{h'}{\cos\theta} \tag{6}$$

2- If the photon enters from the detector's side$^+_1$ (or side$^-_1$), it may emerge from its bottom$_2$, from its side$_2$, or from its top$^+$ (or top$^-$) surface. The distances traveled by the photon in these cases are given by the following equations:

$$d_3 = \frac{h'+L}{\cos\theta} - \frac{R_i}{\sin\theta},\ d_4 = \frac{R_\circ - R_i}{\sin\theta} \text{ and } d_5 = -\frac{K-h'}{\cos\theta} - \frac{R_i}{\sin\theta} \tag{7}$$

The steps of the polar angles (θ) are declared in [1]. The azimuthal angle (ϕ) takes always the value 2π for all values of the polar angle θ. Taking these situations into consideration, the final expression for equation (2) depends on the relation between (θ_2) and (θ_3) as shown in (Fig. 2), and we have two sub-cases discussed as follow:

The Axial Point Source lies in Zone- I ($\theta_3 < \theta_2$)

Equation (2) turns to be $\bar{d} = \frac{I_1}{I_2}$, where I_1 is given as;

$$I_1 = \int_0^{\theta_3} d_1 \sin\theta d\theta + \int_{\theta_3}^{\theta_2} d_3 \sin\theta d\theta + \int_{\theta_2}^{\theta_4} d_4 \sin\theta d\theta + \int_{\theta_4}^{\theta_5} d_5 \sin\theta d\theta \tag{8}$$

The Axial Point Source lies in Zone- III ($\theta_3 > \theta_2$)

In this case, I_1 is given as;

$$I_1 = \int_0^{\theta_2} d_1 \sin\theta d\theta + \int_{\theta_2}^{\theta_3} d_2 \sin\theta d\theta + \int_{\theta_3}^{\theta_4} d_4 \sin\theta d\theta + \int_{\theta_4}^{\theta_5} d_5 \sin\theta d\theta \tag{9}$$

In the two sub-cases, I_2 is given as;

$$I_2 = \int_0^{\theta_5} \sin\theta\, d\theta = (1-\cos\theta_5) \tag{10}$$

The Case of a Non-Axial Point Source

If an arbitrarily positioned isotropic radiating point source is placed at a lateral distance ρ from the axis of the detector, see (Fig. 3). Each striking photon may enter from the detector's bottom$_1$ or from the detector's side$^+_1$ (or side$^-_1$). The two cases are described as:

1- If the photon enters from the detector's bottom$_1$, it may emerge from its bottom$_2$ or from its side$_2$, the distances traveled by the photon in both cases are given by the following equations:

$$d_1 = \frac{L}{\cos\theta} \quad \text{and} \quad d_2 = \frac{\rho\cos\phi + \sqrt{R_\circ^2 - \rho^2\sin^2\phi}}{\sin\theta} - \frac{h'}{\cos\theta} \tag{11}$$

2- If the photon enters from detector's side$^+_1$ (or side$^-_1$), it may emerge from its bottom$_2$, from its side$_2$, or from its top$^+$ (or top$^-$) surface. The distances traveled by the photon in these cases are given by the following equations:

$$d_3^{\pm} = \frac{h'+L}{\cos\theta} - \frac{\sqrt{R_i^2 + \rho^2 \pm 2R_i\rho\cos\phi}}{\sin\theta},\ d_4 = \frac{R_\circ - R_i}{\sin\theta} \text{ and } d_5^{\pm} = -\frac{K+h'}{\cos\theta} - \frac{\sqrt{R_i^2 + \rho^2 \pm 2R_i\rho\cos\phi}}{\sin\theta} \tag{12}$$

The steps of the polar angle θ and the corresponding values of the azimuthal angles ϕ are also declared in [1]. There will be three sub-cases according to the previous situations for getting the final expression of equation (2), described as follow:

The Non-Axial Point Source lies in Zone-I $\left(\theta_3^{\pm} < \theta_2^{\pm}\right)$

Equation (2) turns to be $\overline{d} = \frac{I_3}{I_4}$, where I_3 is given as;

$$\begin{aligned} I_3 = {} & 2\pi \int_0^{\theta^-_3} d_1 \sin\theta\, d\theta + 2\int_{\theta_3^-}^{\theta_3^+} \phi_{\max}(h')\, d_1 \sin\theta\, d\theta + \int_{\theta_3^+}^{\theta_2^+}\int_0^{\pi} d^+_3 \sin\theta\, d\theta\, d\phi + \int_{\theta_3^-}^{\theta_2^-}\int_0^{\pi} d^-_3 \sin\theta\, d\theta\, d\phi \\ & + \pi\left(\int_{\theta_2^+}^{\theta_4^+} d_4 \sin\theta\, d\theta + \int_{\theta_2^-}^{\theta_4^-} d_4 \sin\theta\, d\theta\right) + \int_{\theta_4^+}^{\theta_5^+}\int_0^{\pi} d^+_5 \sin\theta\, d\theta\, d\phi + \int_{\theta_4^-}^{\theta_5^-}\int_0^{\pi} d^-_5 \sin\theta\, d\theta\, d\phi \end{aligned} \tag{13}$$

The Non-Axial Point Source lies in Zone-II $(\theta_3^+ > \theta_2^+ \text{and} \theta_3^- < \theta_2^-)$

Equation (2) turns to be $\overline{d} = \frac{I_3}{I_4}$, where I_3 is given as;

$$\begin{aligned} I_3 = {} & 2\pi \int_0^{\theta^-_3} d_1 \sin\theta d\theta + 2\int_{\theta_3^-}^{\theta_2^+} \phi_{\max}(h') d_1 \sin\theta d\theta + \int_{\theta_3^-}^{\theta_2^-}\int_0^{\pi} d_2 \sin\theta d\theta d\phi + 2\int_{\theta_2^+}^{\theta_3^+}\int_0^{\phi_{\max}(h')} d_2 \sin\theta d\phi d\theta \\ & + \pi\left(\int_{\theta_3^+}^{\theta_4^+} d_4 \sin\theta d\theta + \int_{\theta_2^-}^{\theta_4^-} d_4 \sin\theta d\theta\right) + \int_{\theta_4^+}^{\theta_5^+}\int_0^{\pi} d^+_5 \sin\theta d\theta d\phi + \int_{\theta_4^-}^{\theta_5^-}\int_0^{\pi} d^-_5 \sin\theta d\theta d\phi \end{aligned} \tag{14}$$

The Non-Axial Point Source lies in Zone-III $\left(\theta_3^{\pm} > \theta_2^{\pm}\right)$

Equation (2) turns to be $\bar{d} = \frac{I_3}{I_4}$, where I_3 is given as;

$$I_3 = 2\pi \int_0^{\theta_3^-} d_1 \sin\theta d\theta + 2\int_{\theta_2^-}^{\theta_3^-}\int_0^{\pi} d_2 \sin\theta d\theta + 2\left(\int_{\theta_2^-}^{\theta_2^+}\left(\phi_{\max}(h'+L)d_1 \sin\theta - \int_0^{\phi_{\max}(h'+L)} d_2 \sin\theta d\phi\right)d\theta\right)$$
$$+2\int_{\theta_3^-}^{\theta_3^+}\int_0^{\phi_{\max}(h')} d_2 \sin\theta d\phi d\theta + \pi\left(\int_{\theta_3^+}^{\theta_4^+} d_4 \sin\theta d\theta + \int_{\theta_3^-}^{\theta_4^-} d_4 \sin\theta d\theta\right) + \int_{\theta_4^+}^{\theta_5^+}\int_0^{\pi} d^+{}_5 \sin\theta d\theta + \int_{\theta_4^-}^{\theta_5^-}\int_0^{\pi} d^-{}_5 \sin\theta d\theta \quad (15)$$

In the last three sub-cases, I_4 is given as;

$$I_4 = 2\pi\left[(1-\cos\theta_3^+) + 0.5(\cos\theta_3^+ - \cos\theta_5^+) + 0.5(\cos\theta_3^- - \cos\theta_5^-)\right] + 2\int_{\theta_3^-}^{\theta_3^+} \phi_{\max}(h')\sin\theta \, d\theta \quad (21)$$

The case of a cylindrical source

The efficiency of a well-type detector arising from a cylindrical source, with radius (S) and height (H) placed at distance (h_o) from the core of the detector is given by equation (22).

$$\varepsilon_{cyl} = \frac{2}{H \quad S^2} \int_{h_o}^{h_0+H} \int_0^{S} \varepsilon_{point} \quad \rho \quad d \quad \rho \quad d\,h \quad (22)$$

In equation (22), (ε) is the full-energy peak efficiencies of an off-axis isotropic radiating point source. The path lengths of the gamma photon through the source container, the absorber, the window material and the detector end-cap are given in [1].

Results

The full energy peak efficiency (ε_p) is calculated using our present approach and tested against the published data for two HPGe well–type detectors of different sizes, with parameters listed in table 1. The calculations are done for energy ranges from several KeV to several MeV, and the related radioactive nuclides are listed in table 1 for the two detectors. The discrepancy between our calculations and the reference data sets is calculated as ($\frac{(\varepsilon_{cal} - \varepsilon_{ref})}{\varepsilon_{cal}}\%$). The source-detector geometries are described as follow:

For the first detector, the efficiency values are calculated in the energy range 0.46- 1.836 MeV for a 5 mL cylindrical source and compared with the results obtained experimentally by Hernández and El-Daoushy [16], in Fig (4). In addition, the efficiency values are calculated for the second detector using two cylindrical sources of 3 and 8 cm^3 and compared with the experimental and simulated data (GEANT code) obtained by Laborie et al., [11, 17], as in Figs (5 and 6), respectively. The discrepancies were less than 3% on average in all cases, while it was 4% as reported in [1, 2].

Table 1
Parameters of the detectors used in the present work and the related radioactive nuclides

Parameters of the detectors (cm)			Radioactive nuclides	
	Detector 1	Detector 2	Detector 1	Detector 2
Crystal Radius	5.3	3.75	^{210}Pb, ^{241}Am, ^{40}K, ^{226}Ra-daughters, ^{60}Co, ^{88}Y, ^{139}Ce	^{210}Pb, ^{241}Am, ^{109}Cd, ^{57}Co, ^{60}Co, ^{88}Y, ^{137}Cs ^{139}Ce ^{203}Hg, ^{54}Mn, 113Sn
Crystal Length	5.8	7.5		
Well Radius	0.5	1		
Well Length	4	5.4		
Window Material	Al	Al		
Window Thickness	0.1	0.05		

Conclusions

The theoretical calculation of the average path length covered by an incident photon and the geometrical solid angle lead to a straightforward mathematical formula to calculate the different efficiencies for the well-type detectors. This approach offers a good method to calibrate the HPGe Well-Type detectors over the entire energy range without the need of using standard sources, as in case of experimental method, nor optimizing the detector parameters as in the Monte Carlo simulations. The new method shows validity more than that by the original direct mathematical method reported in [1, 2] as it reduces the discrepancies with the experimental method to less than 3% for extended sources in the case of the calculation of the (ε_p). For comparison, the best accuracy using the Monte Carlo simulations was less than 5% by optimizing the detector parameters.

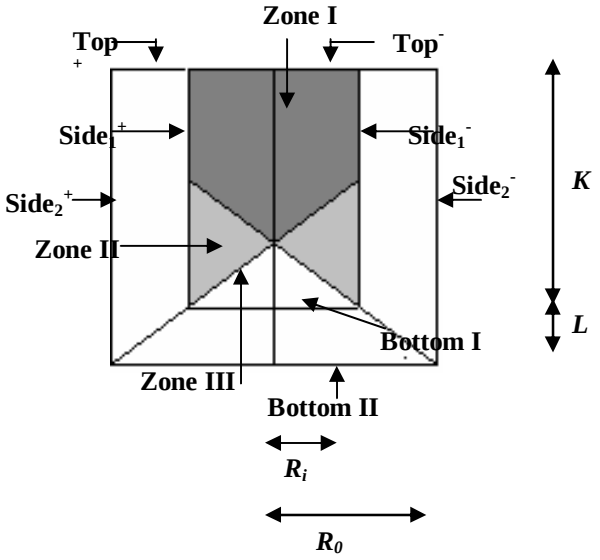

Fig. 1. Schematic diagram of a well-type detector.

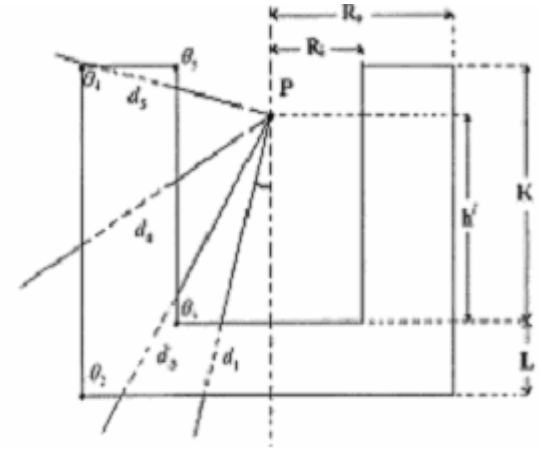

Fig. 2. An axial Point Source.

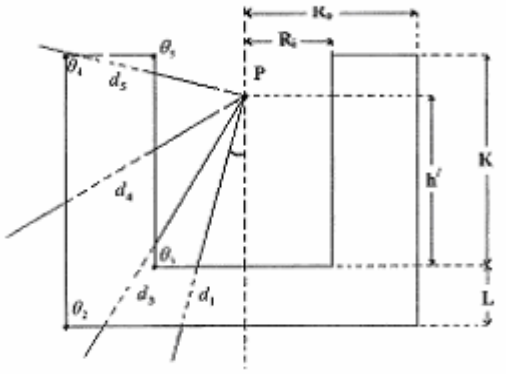

Fig. 3. Non-axial axial Point Source.

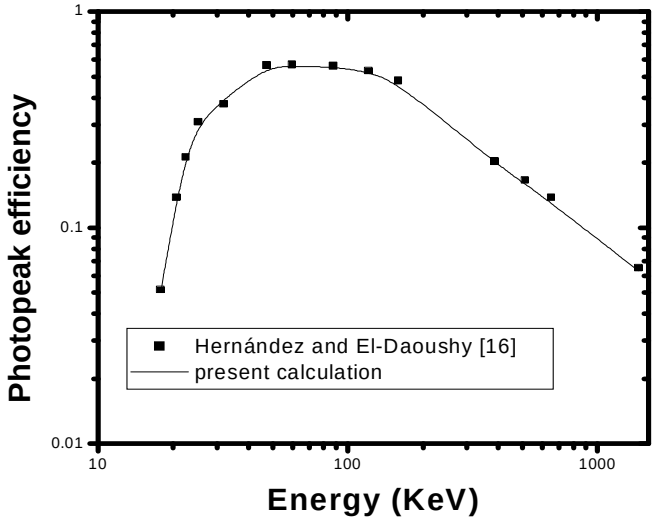

Fig. 4. Photopeak efficiency for a cylindrical source in the case of a HPGe well detector; squares represent the experimental work in [16], solid line represents the calculated efficiency values using the present approach.

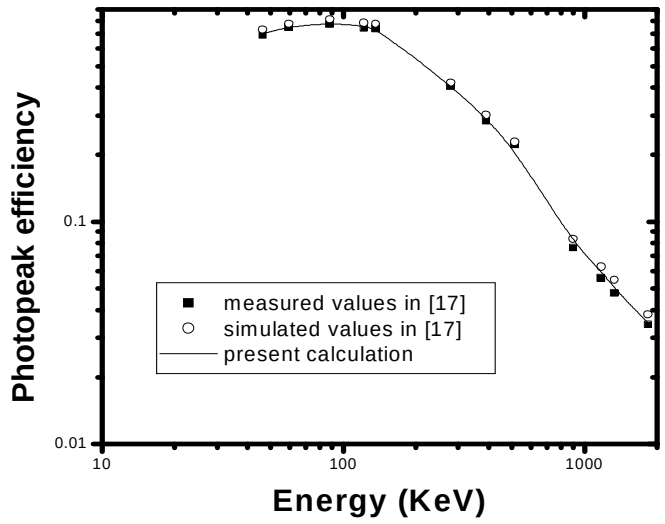

Fig. 5. Photopeak efficiency for a 3 cm^3 cylindrical source with a HPGe well detector; squares and circles represent the experimental and simulated work in [17], solid line represents the calculated efficiency values using the present approach.

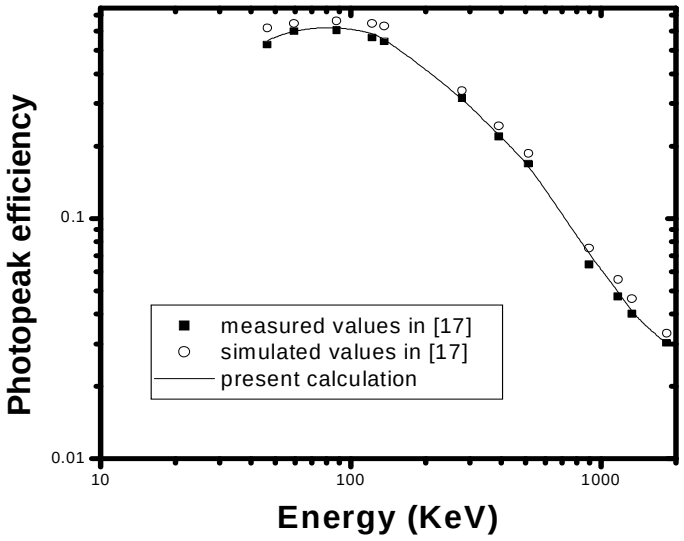

Fig. 6. Photopeak efficiency for a 8 cm^3 cylindrical source with a HPGe well detector; squares and circles represent the experimental and simulated work in [17], solid line represents the calculated efficiency values using the present approach.

References

[1] Abbas, M. I. 2001. Appl. Radiat. Isot. 54, 761-768.

[2] Abbas, M. I., Selim, Y. S., 2002. Nucl. Instr. and Meth. A 480, 651-657.

[3] Jeronymo, J. M. F., Mani, G. S., Delaunay-Olkowsky, J., Sadeghi, A., Williamson, C. F., 1963. Nucl. Physics. 47, 157.

[4] Redon, D., Mani, G. S., Delaunay-Olkowsky, J., Williamson, C. F., 1964. Nucl. Instr. and Math. 26, 18-21.

[5] Snyder, B. J., 1965. Ph.D. Dissertation, Michigan University, USA.

[6] Decombaz, M., Laedermann, J. P., 1996., Nucl. Instr. and Math. A 369, 375-379.

[7] Sima, O., Arnold, D., 1996. Appl. Radiat. Isot. 47, 889-893.

[8] Sima, O., 2000. Nucl, Instr. and Math. A 450, 98-108.

[9] Blaauw, M., 1998., Nucl. Instr. and Math. A 419, 146-153.

[10] Wang, T. K., Hou, I. M., Tseng, C. L., 1999. Nucl. Instr. and Math. A 425, 425-515.

[11] Laborie, J. M., Le Petit, G., Abt, D., Girard, M., 2000. Appl. Radiat. Isot. 53, 57-62.

[12] Selim, Y. S., Abbas, M. I., 1994. Radiat. Phys. Chem. 44 (1), 1-4.

[13] Selim, Y., S., Abbas, M., I., 1995. Egypt. J. of Phys. 26, 79-89.

[14] Abbas, M. I., Younis,Y. S., 2000. Egypt. J. Phys. 2, 151.

[15] Hubbell, J. H., Seltzer, S. M., 1995. NISTIR 5632, U. S. A.

[16] Hernández, F., and El-Daoushy, F., 2003. Nucl. Instr. and Meth. A 498, 340-351.

[17] Laborie, J. M., Le Petit, G., Abt, D., Girard, M., 2002. Nucl. Instr. And Meth. A 479, 618-630.